https://doi.org/10.5194/egusphere-2026-6250
Preprint. Discussion started: 9 November 2026
© Author(s) 2026. CC BY 4.0 License.

Melt Feedback of Greenland Supraglacial Lakes at Catchment Scale

Jiake Wu[1, 2], Lei Zheng[1, 2], Qi Liang[1, 2], Teng Li[1, 2], Xiao Cheng[1, 2], Fengming Hui[1, 2]

[1]School of Geospatial Engineering and Science, Sun Yat-sen University & Southern Marine Science and Engineering Guangdong Laboratory (Zhuhai), Zhuhai 519082, China.
[2]Key Laboratory of Comprehensive Observation of Polar Environment (Sun Yat-sen University), Ministry of Education, Zhuhai 519082, China

Correspondence to: Lei Zheng (zhenglei6@mail.sysu.edu.cn) and Fengming Hui (huifm@mail.sysu.edu.cn)

Abstract. Supraglacial lakes (SGLs) are ubiquitous along the margins of the Greenland Ice Sheet (GrIS) during summer. By absorbing and storing energy and facilitating heat exchange between the atmosphere, lake water, and underlying ice, SGLs enhance lake-bottom ablation and contribute to ice-sheet mass loss. However, this potentially important contribution remains poorly quantified due to the lack of lake-bottom ablation observations. In this study, we estimated lake-bottom ablation of SGLs on the GrIS and the associated melt feedback using a distributed SGL model evaluated against satellite observations. Experiments in typical catchments reveal that the lake-bottom ablation volumes ranged from 2-6×10^{-3} km^3 and the maximum rate reached 160 mm day^{-1}. Lake-bottom ablation rates increased exponentially with rising air temperature and responded more rapidly than surrounding firn/ice melt rates. Lake-bottom ablation contributed more than 30% of the lake volume growth, and SGL melt feedbacks increased the mean catchment melt rate by 12%-19% relative to the all-ice baseline. Our findings emphasize the critical role of lake-bottom ablation in amplifying surface melt over the GrIS under continued climate warming.

1 Introduction

The polar ice sheets have undergone pronounced mass loss over recent decades in response to climate warming (Hanna et al., 2021; Otosaka et al., 2023; The IMBIE Team, 2020). Recent mass loss of the Greenland ice sheets (GrIS) is increasingly controlled by enhanced surface melting (van den Broeke et al., 2017; Enderlin et al., 2014; Zheng et al., 2025), which generates substantial meltwater runoff and promotes the development of extensive supraglacial hydrological systems, including supraglacial lakes (SGLs).

During the melt season, SGLs are predominantly distributed below 1600 m elevation on the GrIS (Fan et al., 2025) and exert control on ice-sheet stability and mass balance. Lakes may drain rapidly within hours to days through hydrofracture, efficiently transferring meltwater and heat from the surface to the bed. Such drainage events reduce basal friction, elevate basal water pressure, and induce transient ice uplift and ice-flow acceleration (Chudley et al., 2019; Hoffman et al., 2011; Morriss et al., 2013; Tedesco et al., 2013). With the resulting strongly perturbed ice-sheet dynamics, this process may further promote the formation of new englacial pathways such as crevasses and moulins and trigger cascading drainage of adjacent

https://doi.org/10.5194/egusphere-2026-6250
Preprint. Discussion started: 9 November 2026
© Author(s) 2026. CC BY 4.0 License.

lakes (Christoffersen et al., 2018; Lutz et al., 2025). In addition, the drainage of SGLs delivers surface microbial communities, organic and inorganic nutrients into subglacial hydrological systems, disrupting local biogeochemical processes and altering subglacial environmental conditions (Lamarche-Gagnon et al., 2019; Musilova et al., 2017; Wadham et al., 2010).

Beyond these impacts, SGLs play a critical role in enhancing ice ablation through their thermal effects. Owing to their lower albedo relative to firn and bare ice, SGLs absorb more solar radiation and act as efficient heat reservoirs, intensifying ablation at the ice-lake interface (Tedesco et al., 2012). Moreover, the stored heat buffers short-term atmospheric cooling, allowing lake-bottom melting to persist even after surface melting ceases (Wu et al., 2025). Together, these processes constitute a positive SGL melt feedback that accelerates mass loss from the GrIS. As Arctic warming intensifies, SGLs have become more numerous, expanded in area, and migrated inland and toward higher elevations (Fan et al., 2025; Howat et al., 2013). Therefore, better constraining lake-bottom ablation is essential for quantifying SGL melt feedbacks and reducing uncertainties in the GrIS mass-loss estimates.

Although lake volumes can be derived from satellite observations (Lutz et al., 2024; Melling et al., 2024; Pope et al., 2016; Zhou et al., 2025), it remains difficult to distinguish whether the observed volume changes originate from lake-bottom ablation or meltwater inputs from the catchment. Consequently, the enhancement of ablation associated with SGLs, as identified statistically by Qiu et al. (2025) for the southwestern GrIS, has not yet been quantitatively assessed. Tedesco et al. (2012) first reported in situ measurements of lake-bottom ablation for two lakes in the western GrIS, with rates of ~6 cm/day (110-135% higher than that of bare ice). Despite the short duration (~5 days), these data have provided crucial baseline information for the development and improvement of SGL models. Lüthje et al. (2006) demonstrated through a 30-day simulation that lake-bottom ablation was 110-170% higher than that of bare ice. However, these advances have been achieved using single-point measurements or one-dimensional models, leaving the spatial distribution of lake-bottom ablation unexplored and its contribution to lake volume unquantified at the real catchment scale.

Here, we (i) apply the distributed SGL model GlacierLake_v3 to simulate lake-bottom ablation and examine its spatial and temporal variability, (ii) explore the relationships between lake-bottom ablation and key meteorological drivers, and (iii) quantify the contribution of lake-bottom ablation to lake volume and the associated SGL melt feedback at the catchment scale.

2 Data and methods

2.1 Study sites

We focus on terminal lakes, a subset of SGLs with no observable outflow channels, which offer a simplified hydrological setting. As they initially contain no water when the melt season begins, the subsequent water volume in these lakes offers a direct estimate of cumulative upstream runoff (Yang et al., 2019). We selected three terminal lakes on the GrIS (Wu et al., 2026), which are located in the southwestern, central-western, and northeastern basins, respectively (Figure 1a). Lake 1

https://doi.org/10.5194/egusphere-2026-6250
Preprint. Discussion started: 9 November 2026
© Author(s) 2026. CC BY 4.0 License.

(66.896N, 48.675W) appeared in 2021, and the area and mean elevation of the corresponding catchment were ~13 km^2 and 1370 m. It is located ~20 km southeast of the KAN_M site from the Programme for Monitoring of the Greenland Ice Sheet (PROMICE), where the annual air temperature is -11°C and the annual runoff is 2.1 m w.e. yr^{-1}. Lake 2 (69.890N, 49.293W) experienced warmer weather conditions (annual air temperature -6°C) and stronger annual runoff (2.8 m w.e. yr^{-1}) in 2020, with a catchment area of ~30 km^2 and a mean elevation of 1190 m. The northernmost Lake 3 (78.83N, 22.985W) was characterized by the lowest annual air temperature (-13°C), the largest catchment (~34 km^2), the lowest mean elevation (730 m), and the weakest annual runoff (1.3 m w.e. yr^{-1}) in 2021. The annual ice velocities within catchments were 146, 370, and 478 m yr^{-1}, respectively. When scaled to the melt-season duration, the associated ice displacement is limited compared to the lake area dimensions; thus, the influence of ice flow is neglected in this study.

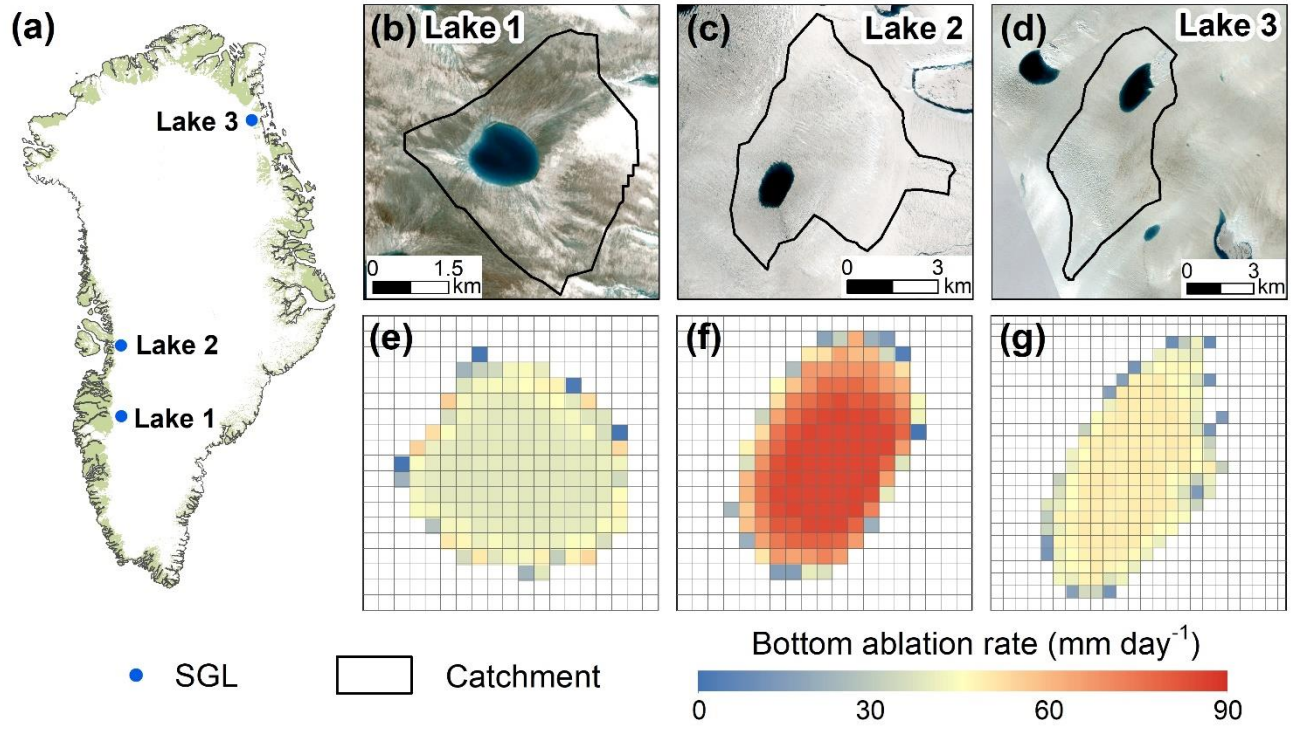


Figure 1. (a) Locations of three terminal lakes (blue dots) across the Greenland Ice Sheet. (b-d) Supraglacial catchments (black outlines) of Lakes 1-3 overlaid on Sentinel-2 imagery acquired on 31 July 2021, 2 August 2020, and 15 August 2021, respectively. (e-g) Spatial distributions of modelled lake-bottom ablation rates from Lakes 1-3, respectively.

2.2 GlacierLake_v3

The distributed SGL model GlacierLake_v3 based on energy balance and phase transition, can simulate the evolution of terminal SGLs (Wu et al., 2026), including meltwater production, routing, loss, filling, and energy transport within meltwater columns. We therefore used GlacierLake_v3 to simulate lake-bottom ablation. The catchments of SGL were extracted from ArcticDEM and were divided into 100×100 m grids. The runoff module simulated meltwater production, and

https://doi.org/10.5194/egusphere-2026-6250
Preprint. Discussion started: 9 November 2026
© Author(s) 2026. CC BY 4.0 License.

meltwater routing toward topographic depressions within the catchment was parameterized using Darcy's Law for snow and Manning's equation for ice surface, respectively. During this process, the loss due to retention, refreezing, evaporation, and so on was represented by the satellite-calibrated meltwater loss rate (Text A1). Accumulated meltwater progressively filled surface depressions, and bare-ice grids are reclassified as lake grids once submerged. For these lake grids, the energy balance is calculated, including shortwave radiation propagation, convection, and heat conduction. The model development was fully described in Wu et al. (2026).

The lake volume from the first valid optical image was used as one of the initial conditions to better constrain the model. The corresponding lake depth was derived following Zhou et al. (2025), in which a machine learning approach combines ICESat-2 data with multispectral imagery and has been shown to provide higher accuracy than traditional physically based methods relying solely on optical data. For Lake 1, model forcing variables, including air temperature, air pressure, wind speed, relative humidity, and downward shortwave and longwave radiation, were obtained at the nearby KAN_M Station provided by the PROMICE (Fausto et al., 2021). For Lakes 2 and 3, these variables were derived from the ERA5 reanalysis due to the absence of in-situ measurements. Precipitation and snowfall were provided by the Regional Atmospheric Climate Model (RACMO2.3p2), specifically designed for polar applications and extensively used in the GrIS climate and surface processes studies (Huai et al., 2022; Noël et al., 2018; Zhang et al., 2025). The data used in this study and simulation settings were provided in Table A1 and Text A1.

GlacierLake_v3 successfully reproduces the evolution of Lakes 1-3. The simulated results are in good agreement with satellite-derived estimates (Figure A1). For lake areas, the R^2 values are 0.68, 0.89, and 0.89, with RMSEs of 5.5% to 8.1%. For lake volumes, the corresponding R^2 values are 0.83, 0.83, and 0.95, with RMSEs ranging from 9.9% to 12%. These results provide confidence in the model for subsequent analysis.

2.3 Supraglacial melt feedbacks

Compared to the surrounding ice-sheet surface, lake-bottom ablation rates exceed bare-ice melt rates by more than 100%, leading to an enhanced mean melt rate within the catchment. To quantify the impact of SGLs on catchment-scale melting, we define the enhancement in mean melt rate ΔM (mm day^{-1}) following Leeson et al. (2015),

$$\Delta M = \frac{M_{ice}A_{ice}+M_{lake}A_{lake}}{A_{total}} - M_{ice}\ , \quad (1)$$

The first term on the right side of Equation (1) represents the area-weighted mean melting rate within the catchment in the presence of an SGL. Here, M_{ice} and M_{lake} are simulated melt rates of bare ice and lake bottom, respectively. A_{lake} is the lake area simulated by GlacierLake_v3, A_{total} is the catchment area, and $A_{ice} = A_{total} - A_{lake}$ is the remaining bare-ice area within the catchment.

The relative strength of the SGL melt feedback is further characterized by the dimensionless index I (%), defined as,

$$I = \frac{\Delta M}{M_{ice}} \times 100\%\ , \quad (2)$$

https://doi.org/10.5194/egusphere-2026-6250
Preprint. Discussion started: 9 November 2026
© Author(s) 2026. CC BY 4.0 License.

which expresses the fractional increase in the catchment-mean melt rate attributable to the presence of SGLs.

3 Result

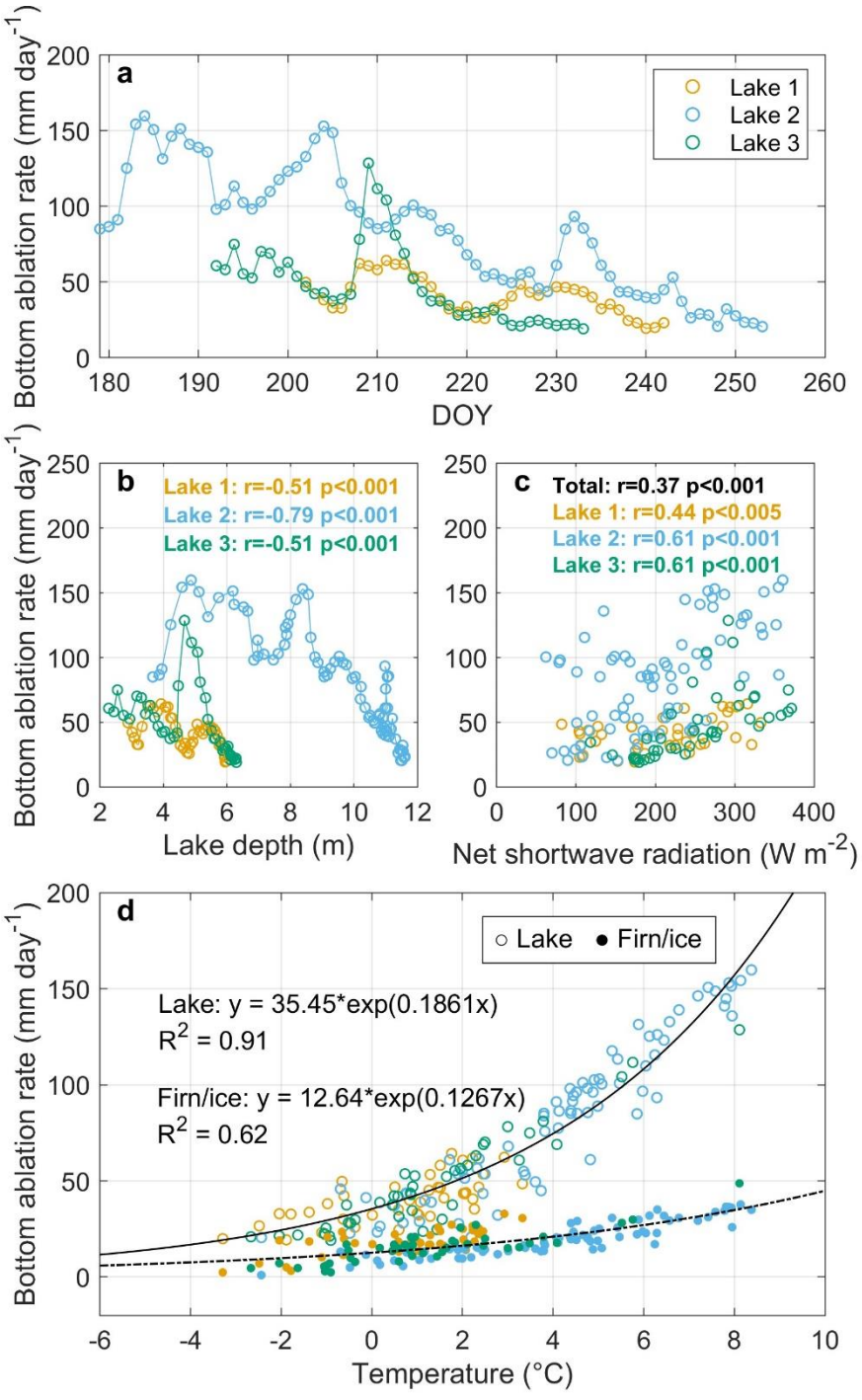
3.1 Spatio-temporal patterns of bottom ablation rate

Daily lake-bottom ablation rate distributions during the simulation are presented in Figure 1e-g. Overall, the rate decreased from the lake center toward the edge. Lake 1 exhibited relatively moderate lake-bottom ablation rates with a mean of 39.1 mm day^{-1}, and showed noticeable spatial heterogeneity near the lake edge, where locally elevated values were modelled (Figure 1e). Lake 3 showed a similar overall magnitude (Figure 1g), but its spatial pattern more closely followed the typical radial pattern. In contrast, Lake 2 exhibited substantially higher lake-bottom ablation rates across a larger portion of the lake bottom (Figure 1f). The mean rate reached 67.8 mm day^{-1}, with a maximum of 85.5 mm day^{-1}, exceeding those of Lake 1 and Lake 3 by more than 1.5 times. The lake-bottom ablation rate negative gradient from the center to the edge was also strongest in Lake 2, markedly greater than in Lake 1 and Lake 3.

The relationship between lake-bottom ablation rate and lake depth for each grid is shown in Figure B1. For all three lakes, lake-bottom ablation rates increased rapidly with increasing depth within the shallow range (0-5 m). Beyond this depth range, the three lakes exhibited distinct behaviors. In Lake 1 and Lake 3, lake-bottom ablation rates reached a maximum and then slightly decreased, gradually approaching constant values of approximately 38 mm day^{-1} and 48 mm day^{-1}, respectively. In contrast, lake-bottom ablation rates in Lake 2 continued to increase with depth until approximately 15 m, beyond which the rates tended to level off at around 85 mm day^{-1}.

The time series of lake-bottom ablation rates from Lakes 1-3 in Figure 2a were derived by averaging over the lakes. Lake 2 showed the highest daily lake-bottom ablation rates (Figure 2), with a mean value of 80.4 mm day^{-1}. The maximum rate reached 159.8 mm day^{-1} on July 2 (DOY 184), with additional pronounced peaks on July 23 (DOY 204) and on August 20 (DOY 232). In contrast, Lake 1 exhibited the lowest lake-bottom ablation rates, averaging 40.7 mm day^{-1}, while Lake 3 showed comparable values to Lake 1, but experienced an extreme event reaching 128.7 mm day^{-1} on July 28 (DOY 209).

https://doi.org/10.5194/egusphere-2026-6250
Preprint. Discussion started: 9 November 2026
© Author(s) 2026. CC BY 4.0 License.



135 **Figure 2. (a) Daily lake-bottom ablation rate variation for Lakes 1-3. Daily lake-bottom ablation rate variation with (b) lake depth and (c) net shortwave radiation increased. (d) Relationship between air temperature and ablation rates for the lake bottom (circle) and firn/ice surface (dot) in the corresponding catchment.**

https://doi.org/10.5194/egusphere-2026-6250
Preprint. Discussion started: 9 November 2026
© Author(s) 2026. CC BY 4.0 License.

3.2 Lake-bottom ablation far more rapidly than the surrounding bare ice

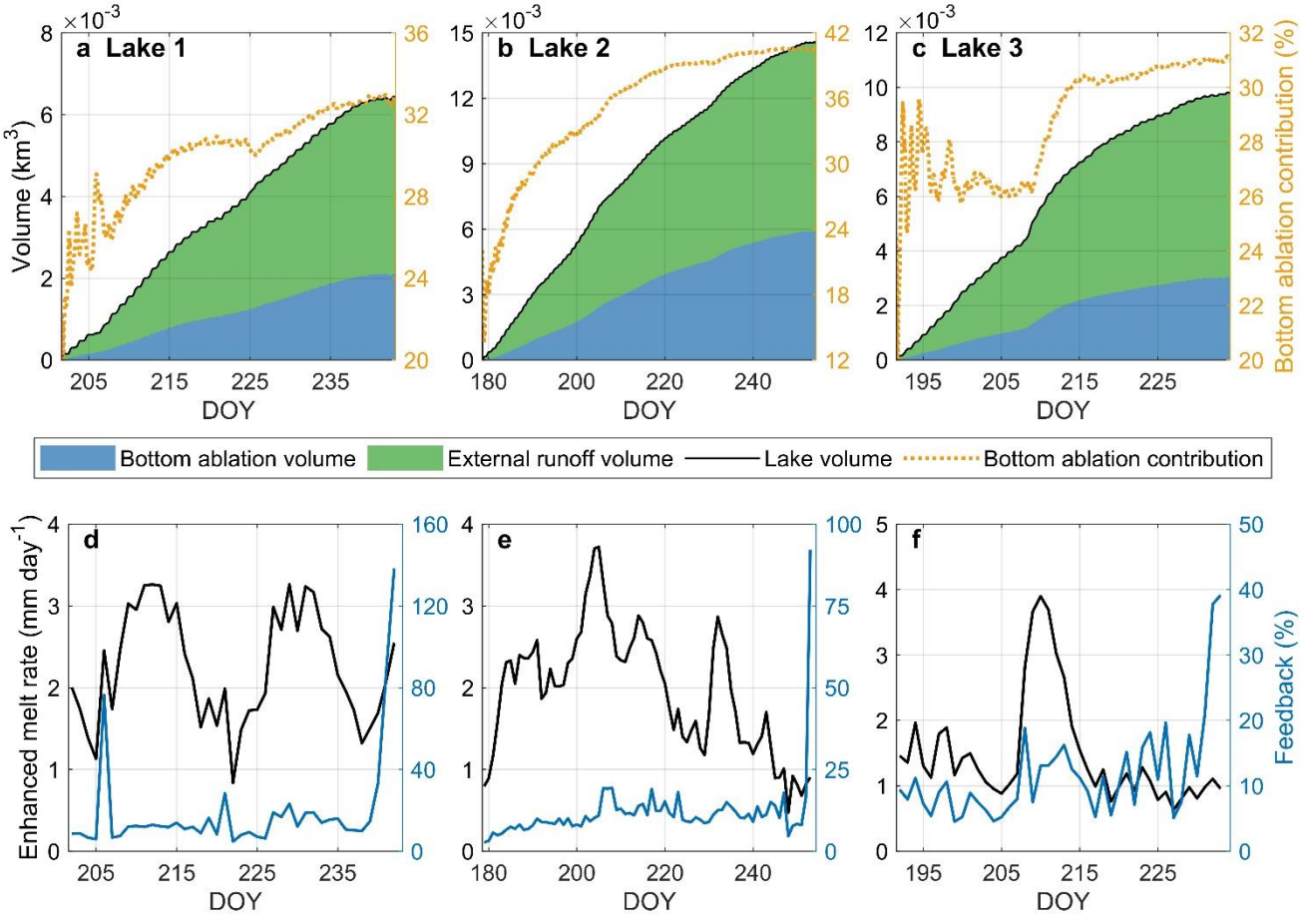
The daily lake-bottom ablation rate variations with mean lake depth, net shortwave radiation, and air temperature were examined in Figure 2b-d. For each lake, there is a significant negative correlation ($r=-0.79$ to -0.51, $p<0.001$) between mean lake depth and lake-bottom ablation rate (Figure 2b). The increase in net shortwave radiation provides energy for the growth of the SGL, and the lake-bottom ablation rate increases accordingly (Figure 2c). The overall relationship was highly scattered, and a weak but statistically significant positive correlation was observed ($r=0.37$, $p<0.001$). When examined for individual lakes, the positive correlation became stronger ($r=0.44$ to 0.61) and remained statistically significant.

Notably, lake-bottom ablation rate increased exponentially with air temperature (Figure 2d). Over the temperature range of -5°C to 10°C, the fitted relationship yielded a high R^2 of 0.91. Within the same range, the firn/ice melt rate in Catchments 1-3 also showed a significant exponential relationship with air temperature, with an R^2 of 0.62. However, firn/ice melt increases much less rapidly with air temperature than lake-bottom ablation. From -5°C to 10°C, the firn/ice melt rate increased from 6.7 to 44.8 mm day^{-1}, while the lake-bottom ablation rate rose from 14 to 228 mm day^{-1}. The difference between the two widened from 7.3 to 183.2 mm day^{-1}.

3.3 Contribution of bottom ablation and SGL melt feedback

The relative contributions of external runoff and lake-bottom ablation to lake volume growth were quantified in Figure 3a-c. Since the initial lake volume was prescribed at the start of the simulation, the volumes shown represent net increase relative to the initial state. The simulation results showed that lake growth was primarily driven by external runoff (>60%), whereas the contribution from lake-bottom ablation increased with lake expansion and exceeded 30% in late August in all three cases. In particular, Lake 2 exhibited a markedly higher contribution from lake-bottom ablation, exceeding 40%, consistent with its higher lake-bottom ablation rates. To further clarify the impact of SGL on the catchment scale, we calculated the enhanced melt rate within catchments and SGL melt feedback (Figure 3d-f). The existence of the lake has led to an average increase of 2.2, 2, and 1.5 mm day^{-1} in the melting rate within Catchments 1-3, respectively, with a maximum of ~4 mm day^{-1} in Catchment 3. The average feedback for the three catchments was 19%, 12%, and 12%, respectively. The feedback was mainly concentrated within 40%, while the maximum for Lakes 1 and 2 reached 138% and 92%, and these extreme values are mainly caused by the extremely low bare-ice melt rate (<5 mm day^{-1}) due to atmospheric cooling.

https://doi.org/10.5194/egusphere-2026-6250
Preprint. Discussion started: 9 November 2026
© Author(s) 2026. CC BY 4.0 License.



165 **Figure 3. Lake volume (black line), external runoff (green area), lake-bottom ablation (blue area), and the contribution of lake-bottom ablation to lake volume (orange dashed line) for Lakes 1-3 (a-c). Enhanced melt rates associated with SGL presence and SGL melt feedbacks for Catchments 1-3 (d-f).**

4 Discussion

4.1 Uncertainties

170 Lake-bottom ablation of SGLs has long been recognized as an important process influencing ice-sheet mass loss (Law et al., 2020; Lüthje et al., 2006; Tedesco et al., 2012). However, a robust quantitative estimation has remained limited, largely due to the challenges of continuously resolving melt rates and their spatial evolution at the lake bottom from both in situ measurements and satellite observations. Here, using the distributed GlacierLake_v3 model, we provided the spatial and temporal variation of lake-bottom ablation from three SGLs across distinct basins, highlighting both local meteorological
175 controls and catchment-scale hydrological influences. Our results bridge this long-standing gap and provide new insights into the role of SGL-bottom ablation in modulating ice-sheet mass balance.

https://doi.org/10.5194/egusphere-2026-6250
Preprint. Discussion started: 9 November 2026
© Author(s) 2026. CC BY 4.0 License.

As the lake deepens during the melt season, its albedo decreases exponentially with increasing depth, which enhances solar energy absorption and, in principle, promotes bottom ablation. However, once the lake depth exceeds ~4 m, the reduction in albedo becomes minimal (Wu et al., 2025), and the associated increase in absorbed energy is insufficient to offset the concurrent reduction in total energy input from atmospheric forcing (Figure B2) in the late melt season. As a result, lake-bottom ablation rate decreases with further increases in lake depth. It should be noted that this analysis focuses on the stage when the lake had already formed and reached a certain size in the simulation.

Although the lake area is more strongly controlled by surface or basal topography (Lampkin and VanderBerg, 2011; Lüthje et al., 2006; Wang and Sugiyama, 2024), the fluctuations in the time-series lake-bottom ablation rate indicated that it is significantly influenced by meteorological factors. Clear geographic contrasts among the selected lakes further support this interpretation, despite the inability to strictly control all variables. Lake 2 occurred at a relatively lower elevation and lay closer to the ice-sheet margin. It experienced the highest air temperature (Figure B2) and correspondingly exhibited the strongest lake-bottom ablation, approximately twice that of Lakes 1 and 3. The lake-bottom ablation rate showed a stronger and more statistically significant relationship with air temperature than with net shortwave radiation (Figure 2c&d).

We presented the lake-bottom ablation contribution and SGL melt feedback in Figure 3. GlacierLake_v3 does not currently incorporate rapid drainage processes, so we assumed that no rapid drainage occurred in any of the three lakes during the simulation period. In reality, however, Lake 1 underwent a rapid drainage event on August 5 (DOY 217), when lake-bottom ablation contributed approximately 22% to the lake volume (Figure 3a), representing a reduction of 11% compared with the no-drainage assumption. Lake 2 also experienced partial drainage later in the simulation. The neglect of drainage events likely led to an overestimation of lake-bottom ablation. Leeson et al. (2015) also took this into account; they performed simulations with a bottom melt rate set at twice the ice-sheet melt rate, which provided an upper-bound estimate. This approach revealed a 0.7%-0.8% increase in surface meltwater volume under the RCP4.5 and RCP8.5 scenarios due to lake-bottom ablation of SGLs on the GrIS. In one-dimensional simulations, SGL melt feedback exceeded 100% (Lüthje et al., 2006; Tedesco et al., 2012; Wu et al., 2025). However, at the catchment scale, this feedback is generally below 100% and often remains within 60% (Figure 3d-f). This difference arises because the feedback is calculated as an area-weighted average over the firn/ice surfaces within the catchment (Equations 1 and 2), effectively representing a regional-mean response rather than a local value.

Other limitations should be noted. The GlacierLake_v3 does not account for lateral energy exchange. At present, lake expansion is represented solely through external runoff input. Furthermore, lake-bottom ablation observations are scarce, limiting the ability to directly validate simulated lake-bottom ablation. Instead, model performance is assessed indirectly through comparisons of lake area and volume. Finally, the simulations are based on a limited number of lakes, and the results may differ or remain uncertain in other regions. Future studies should incorporate rapid drainage processes and expand simulations from individual lakes to broader regional scales.

https://doi.org/10.5194/egusphere-2026-6250
Preprint. Discussion started: 9 November 2026
© Author(s) 2026. CC BY 4.0 License.

4.2 Sensitivity experiments

The melt rates from firn/ice and the lake bottom both increase exponentially with the rising temperature (Figure 2d). Previous studies have shown that surface melt over firn/ice exhibits a well-documented nonlinear dependence on temperature (Graversen et al., 2024; Thompson-Munson et al., 2024; Trusel et al., 2018). It is worth noting that lake-bottom ablation rate increases more rapidly, suggesting a potentially higher sensitivity to temperature changes. We therefore conducted sensitivity experiments by perturbing air temperature (T±1°C) and downward shortwave radiation (S±10%), and compared the relative changes in melt volume between lake-bottom ablation and firn/ice melt within the catchments (Figure 4a). Under S±10% perturbations, the relative changes in melt volume were approximately 10-15% for both lake-bottom ablation and firn/ice melt. In contrast, under T±1°C perturbations, lake-bottom ablation exhibited a larger response (15-30%) than the firn/ice melt (<10%) within catchments. Because lake-bottom ablation is driven by the temperature difference between the lake water and the underlying ice, we further examined the lake energy budget. Energy inputs include surface shortwave absorption, shortwave penetration, and turbulent convection across the upper and lower lake boundaries. For analysis, we grouped surface energy balance and shortwave penetration as shortwave-radiation-dominated contributions, and upper-boundary turbulent convection as an air-temperature-dominated contribution. Shortwave radiation was the primary energy source for Lakes 1 and 3, with upper-boundary turbulent convection providing an additional positive contribution (Figure 4b&4d). In contrast, turbulent convection contributed more energy than shortwave radiation in Lake 2 (Figure 4c). This is because higher air temperatures over the Lake 2 catchment (Figure B2a) enhanced upper-boundary turbulent convection according to Equation A1, making it the dominant energy source. A similar response occurred in Lake 3, where turbulent convection increased sharply with rising air temperature during DOY 207-211 (Figure B2a). Sensitivity experiments further confirmed the stronger influence of air temperature on lake energy input: T+1°C produced a greater energy increase in upper-boundary turbulent convection than S+10% (Figure 4e-4g). This helps explain why lake-bottom ablation is more sensitive to warming than surrounding firn/ice melt. The 4/3 power dependence in Equation A1 indicates a nonlinear increase in turbulent convection with the temperature difference. Consequently, SGLs may amplify melt responses to atmospheric warming, potentially accelerating ice-sheet mass loss under future warming.

https://doi.org/10.5194/egusphere-2026-6250
Preprint. Discussion started: 9 November 2026
© Author(s) 2026. CC BY 4.0 License.

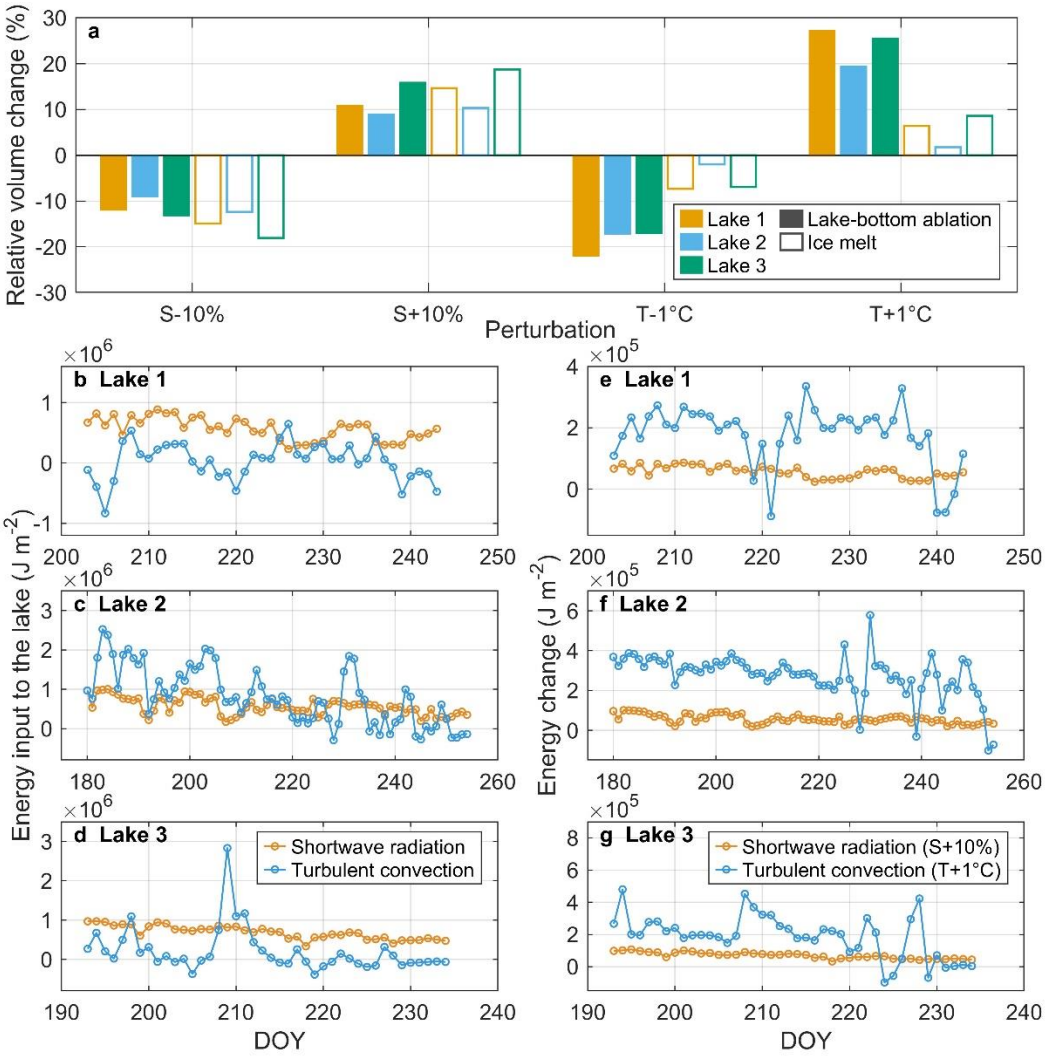


Figure 4. (a) Relative changes in melt volume from lake-bottom ablation (filled bars) and firn/ice melt within the catchments (open bars) in response to perturbations in downward shortwave radiation (S ± 10%) and air temperature (T ± 1 °C). (b-d) The energy contributions from shortwave radiation (surface energy balance and shortwave propagation) and upper-boundary turbulent convection. Positive and negative values indicate energy input to and loss from the lake, respectively. (e-g) Responses of the two energy contributions to perturbations in downward shortwave radiation and air temperature.

5 Conclusion

In this study, we employed the distributed GlacierLake_v3 model to simulate lake-bottom ablation in the GrIS SGLs and to quantify its melt feedback. The mean lake-bottom ablation rate can reach 40-80 mm day^{-1}, with a maximum of 160 mm day^{-1}. The lake-bottom ablation rate exhibits an exponential amplification with air temperature (R^2=0.91), with a much stronger and more robust temperature sensitivity than the firn/ice melt rate. Meltwater surrounding SGLs within the catchment is the primary contributor to lake volume, and lake-bottom ablation accounted for over 30% of total lake growth, indicating that it

https://doi.org/10.5194/egusphere-2026-6250
Preprint. Discussion started: 9 November 2026
© Author(s) 2026. CC BY 4.0 License.

should not be neglected in SGL evolution studies. At typical catchments, the mean SGL melt feedback in summer ranges from 12% to 19%. In extreme cases, particularly toward the end of the melt season when surface melt becomes negligible, the feedback can be substantially amplified, exceeding 100%. The lake energy budget analysis revealed that shortwave radiation was the primary energy source for lake-bottom ablation. However, under warmer conditions, enhanced upper-boundary turbulent convection could exceed the contribution from shortwave radiation, highlighting the potential for atmospheric warming to intensify lake-bottom ablation and amplify melt responses across SGL catchments. Our results provide a quantitative assessment of lake-bottom ablation for individual lakes on the two-dimensional scale, and offer an improved understanding of the role of lake-bottom ablation in SGL evolution and melt feedback, and ice-sheet mass balance.

Appendix A

Text A1. Model settings

The turbulent convection (Q_c, W m^{-2}) at upper and lower lake boundaries is as follows (Buzzard et al., 2018),

$$Q_c(T^*) = sgn(\bar{T} - T^*)\rho_{water}C_{water}J|\bar{T} - T^*|^{4/3}, \quad \text{(A1)}$$

where $\bar{T}$ and T^* are the average lake temperature and the boundary temperature, respectively. ρ_{water} is the density of water, C_{water} is the specific heat capacity, and J is the turbulent heat flux factor.

Meltwater losses during transport are represented by catchment-specific meltwater loss rates, which were calibrated using satellite-derived lake area and volume as reference observations for 2015, 2019, and 2016 for Lakes 1-3, respectively. Calibration involved a two-step parameter search, with R^2 used to evaluate the agreement between simulated and observed lake area and volume. The optimal meltwater loss rate was selected based on the intersection of the two R^2 curves (lake area and volume), ensuring a balanced fit to both variables. A finer search around the initial optimum was then performed to refine the calibrated value. The detailed calibration procedure was described in Wu et al. (2026). These rates were then applied to simulate lake evolution in 2021, 2020, and 2021 for Lakes 1-3, respectively. The model run started on July 21, 2021, June 27, 2020, and July 11, 2021, respectively, which correspond to the acquisition dates of the first valid image. In the simulations, rapid drainage was assumed not to occur, and each simulation ended when the lake surface refroze. The model was validated against satellite-derived lake area and volume, showing good agreement between the simulations and observations (Figure A1).

https://doi.org/10.5194/egusphere-2026-6250
Preprint. Discussion started: 9 November 2026
© Author(s) 2026. CC BY 4.0 License.

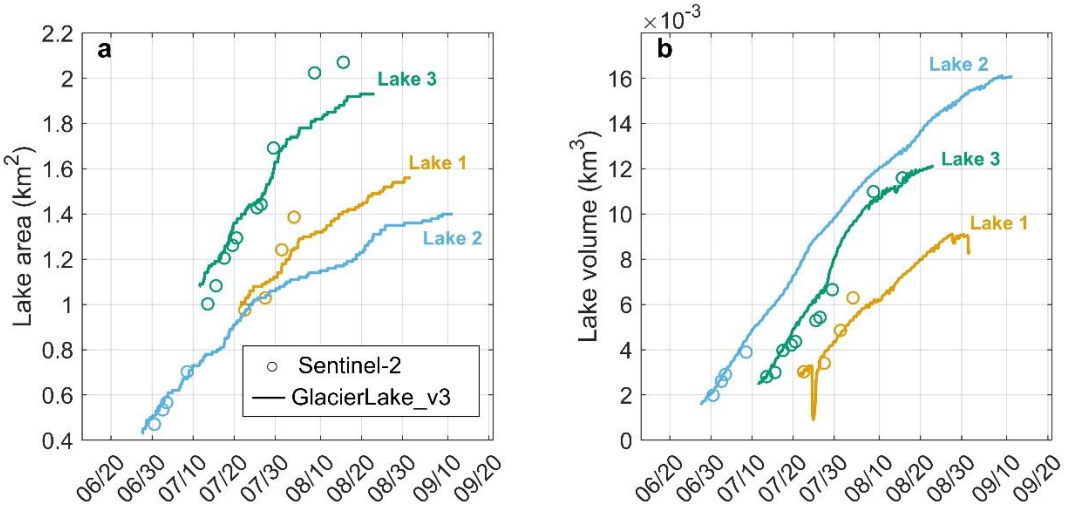


Figure A1. Simulated (solid lines) versus satellite-derived (circles) lake areas and volumes for Lakes 1-3.

Table A1. Datasets for validation and model settings in this study.

Lake	ArcticDEM	Sentinel-2	Forcing data	Simulation period	Meltwater loss rate
1	SETSM_s2s041_WV01_20211005_10200100B7E13800_10200100B9DAD400_2m_lsf_seg1	S2B_MSIL1C_20210721T144759_N0500_R082_T22WFV_20230128T140102 S2A_MSIL1C_20210722T150911_N0500_R025_T22WEV_20230126T172920 S2B_MSIL1C_20210727T150759_N0500_R025_T22WEV_20230126T101004 S2B_MSIL1C_20210731T144749_N0500_R082_T22WFV_20230202T180648 S2B_MSIL1C_20210803T145759_N0500_R125_T22WEV_20230113T215324	PROMICE	2021.7.21-2021.9.1	50%
2	SETSM_s2s041_WV01_20200519_10200100954CB400_10200100987C8600_2m_lsf_seg1	S2A_MSIL1C_20200627T150921_N0500_R025_T22WEC_20230329T234721 S2A_MSIL1C_20200630T151911_N0500_R068_T22WEC_20230404T231817 S2B_MSIL1C_20200702T150759_N0500_R025_T22WEC_20230320T115533 S2A_MSIL1C_20200703T152911_N0500_R111_T22WEC_20230321T050602 S2B_MSIL1C_20200708T152809_N0500_R111_T22WEC_20230317T150859	ERA5	2020.6.27-2020.9.12	80%
3	SETSM_s2s041_WV02_20210519_10300100BE6A3200_10300100BEBDDE00_2m_lsf_seg1	S2A_MSIL1C_20210711T153911_N0500_R011_T26XNN_20230224T073748 S2B_MSIL1C_20210713T152809_N0500_R111_T26XNN_20230122T201355 S2A_MSIL1C_20210715T151911_N0500_R068_T26XNN_20230308T104658 S2A_MSIL1C_20210717T155911_N0500_R097_T26XNN_20230128T022600 S2B_MSIL1C_20210719T154819_N0500_R054_T26XNN_20230122T100457 S2B_MSIL1C_20210720T151809_N0500_R068_T26XNN_20230126T161423 S2A_MSIL1C_20210725T151911_N0500_R068_T26XNN_20230126T180749 S2B_MSIL1C_20210726T153809_N0500_R011_T26XNN_20230527T044449 S2B_MSIL1C_20210729T154819_N0500_R054_T26XNN_20230123T072525 S2B_MSIL1C_20210808T154809_N0500_R054_T26XNN_20230116T183503 S2B_MSIL1C_20210815T153809_N0500_R011_T26XNN_20230526T130624	ERA5	2021.7.11-2021.8.23	67%

https://doi.org/10.5194/egusphere-2026-6250
Preprint. Discussion started: 9 November 2026
© Author(s) 2026. CC BY 4.0 License.

https://doi.org/10.5194/egusphere-2026-6250
Preprint. Discussion started: 9 November 2026
© Author(s) 2026. CC BY 4.0 License.

Appendix B

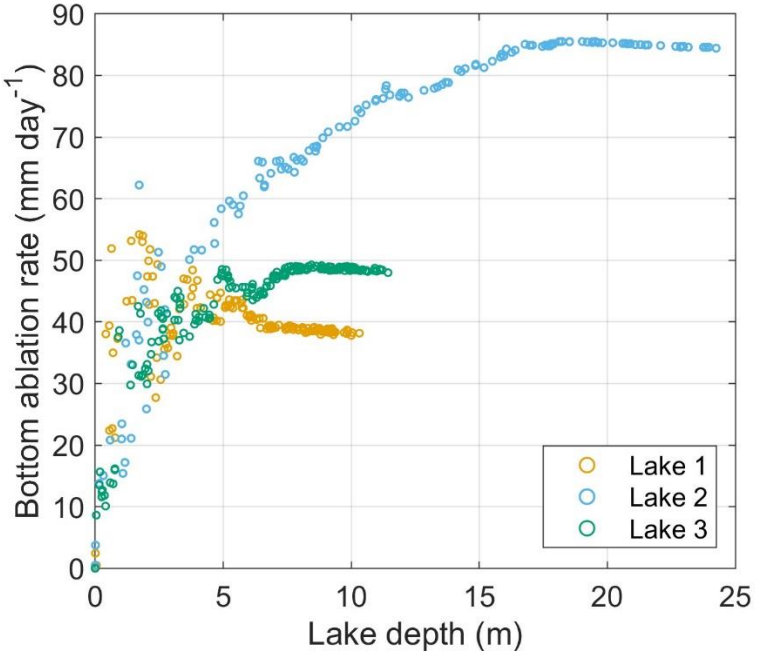


Figure B1. The grid-to-grid relationship between bottom ablation rate and maximum lake depth in Figure 1e-f.

https://doi.org/10.5194/egusphere-2026-6250
Preprint. Discussion started: 9 November 2026
© Author(s) 2026. CC BY 4.0 License.

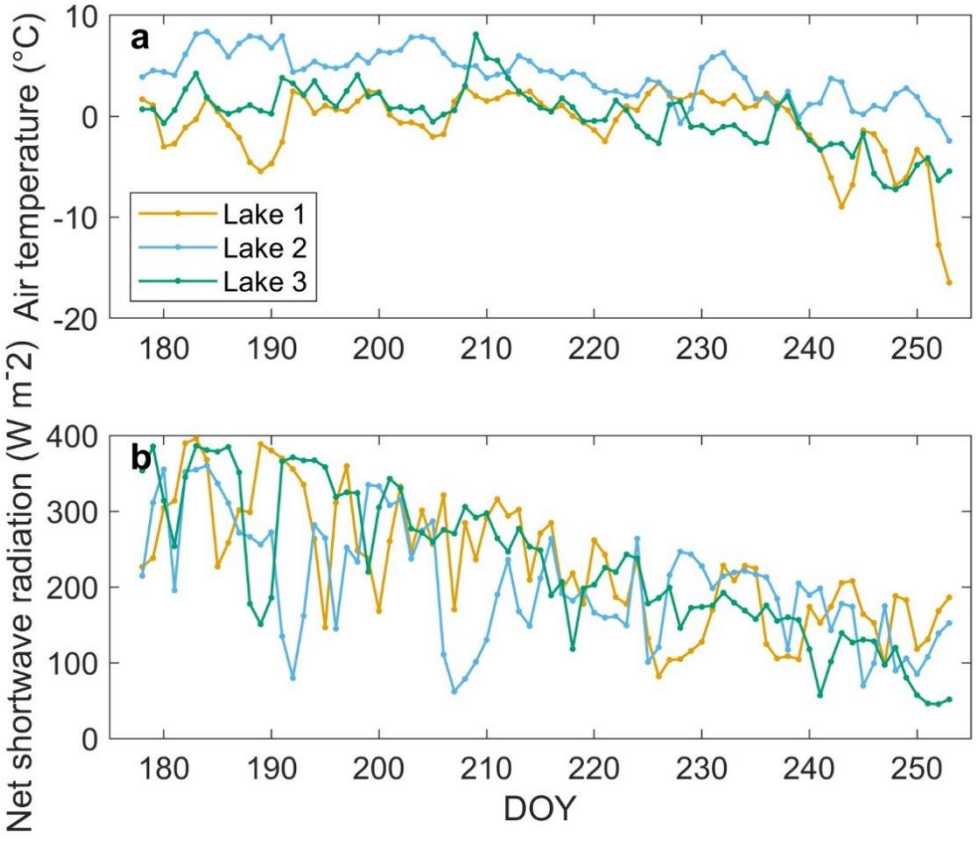


Figure B2. The time series of (a) air temperature and (b) net shortwave radiation for Lakes 1-3.

Code and data availability

The atmospheric observations are obtained from the European Centre for Medium-Range Weather Forecasts for the ERA5 reanalysis data (https://cds.climate.copernicus.eu/datasets/reanalysis-era5-single-levels?tab=overview, last access: July 17, 2025) and the Programme for Monitoring of the Greenland Ice Sheet weather station network (https://dataverse.geus.dk/dataset.xhtml?persistentId=doi:10.22008/FK2/IW73UU, last access: July 20, 2023). The ArcticDEM data are downloaded from https://data.pgc.umn.edu/elev/dem/setsm/ArcticDEM/strips/s2s041/2m/, accessed on July 9, 2025. The Sentinel-1/2 images are downloaded from https://dataspace.copernicus.eu/, accessed on March 22, 2026. The code for the GlacierLake_v3 model is available at https://github.com/Jiake404/GlacierLake_v3/releases/tag/v1.0. The data used in this study and the code for the figures are available at https://github.com/Jiake404/Melt-Albedo-Feedback/releases/tag/v1.0.

https://doi.org/10.5194/egusphere-2026-6250
Preprint. Discussion started: 9 November 2026
© Author(s) 2026. CC BY 4.0 License.

Author contributions

JW performed the simulations, analyzed the results, and wrote the manuscript. LZ helped to develop the ideas and methods, contributed to the validation, and provided funding support. QL and TL assisted with the XGBoost algorithm and discussed the results. XC and FH contributed to the conceptualization and development of the ideas. All authors were involved in editing the manuscript.

Competing interests

The authors declare that they have no conflict of interest.

Acknowledgements

The authors gratefully acknowledge the European Centre for Medium-Range Weather Forecasts (ECMWF) for the ERA5 reanalysis, the Programme for Monitoring of the Greenland Ice Sheet (PROMICE) for the weather station observations, and the Polar Geospatial Center for providing the ArcticDEM data, and the European Space Agency (ESA) for providing Sentinel-1 and Sentinel-2 data. We are grateful to Dr. Brice Noël (University of Liège) for providing the RACMO2.3p2 dataset.

Financial support

This study was supported by the National Natural Science Foundation of China (Grant No. 42422606).

Review statement

The review statement will be added by Copernicus Publications listing the handling editor as well as all contributing referees according to their status anonymous or identified.

References

van den Broeke, M., Box, J., Fettweis, X., Hanna, E., Noël, B., Tedesco, M., van As, D., van de Berg, W. J., and van Kampenhout, L.: Greenland Ice Sheet Surface Mass Loss: Recent Developments in Observation and Modeling, Curr. Clim. Change Rep., 3, 345–356, https://doi.org/10.1007/s40641-017-0084-8, 2017.

Buzzard, S. C., Feltham, D. L., and Flocco, D.: A Mathematical Model of Melt Lake Development on an Ice Shelf, J. Adv. Model. Earth Syst., 10, 262–283, https://doi.org/10.1002/2017MS001155, 2018.

https://doi.org/10.5194/egusphere-2026-6250
Preprint. Discussion started: 9 November 2026
© Author(s) 2026. CC BY 4.0 License.

Christoffersen, P., Bougamont, M., Hubbard, A., Doyle, S. H., Grigsby, S., and Pettersson, R.: Cascading lake drainage on the Greenland Ice Sheet triggered by tensile shock and fracture, Nat. Commun., 9, 1064, https://doi.org/10.1038/s41467-018-03420-8, 2018.

Chudley, T. R., Christoffersen, P., Doyle, S. H., Bougamont, M., Schoonman, C. M., Hubbard, B., and James, M. R.: Supraglacial lake drainage at a fast-flowing Greenlandic outlet glacier, Proc. Natl. Acad. Sci. U.S.A., 116, 25468–25477, https://doi.org/10.1073/pnas.1913685116, 2019.

Enderlin, E. M., Howat, I. M., Jeong, S., Noh, M.-J., van Angelen, J. H., and van den Broeke, M. R.: An improved mass budget for the Greenland ice sheet, Geophys. Res. Lett., 41, 866–872, https://doi.org/10.1002/2013GL059010, 2014.

Fan, Y., Ke, C.-Q., Luo, L., Shen, X., Livingstone, S. J., and Lea, J. M.: Expansion of supraglacial lake area, volume and extent on the Greenland ice sheet from 1985 to 2023, J. Glaciol., 71, 1–13, https://doi.org/10.1017/jog.2024.87, 2025.

Fausto, R. S., van As, D., Mankoff, K. D., Vandecrux, B., Citterio, M., Ahlstrøm, A. P., Andersen, S. B., Colgan, W., Karlsson, N. B., Kjeldsen, K. K., Korsgaard, N. J., Larsen, S. H., Nielsen, S., Pedersen, A. Ø., Shields, C. L., Solgaard, A. M., and Box, J. E.: Programme for Monitoring of the Greenland Ice Sheet (PROMICE) automatic weather station data, Earth Syst. Sci. Data., 13, 3819–3845, https://doi.org/10.5194/essd-13-3819-2021, 2021.

Graversen, R. G., Heiskanen, T., Bintanja, R., and Goelzer, H.: Abrupt increase in Greenland melt enhanced by atmospheric wave changes, Clim Dyn, 62, 7171–7183, https://doi.org/10.1007/s00382-024-07271-6, 2024.

Hanna, E., Cappelen, J., Fettweis, X., Mernild, S. H., Mote, T. L., Mottram, R., Steffen, K., Ballinger, T. J., and Hall, R. J.: Greenland surface air temperature changes from 1981 to 2019 and implications for ice-sheet melt and mass-balance change, Int. J. Climatol., 41, E1336–E1352, https://doi.org/10.1002/joc.6771, 2021.

Hoffman, M. J., Catania, G. A., Neumann, T. A., Andrews, L. C., and Rumrill, J. A.: Links between acceleration, melting, and supraglacial lake drainage of the western Greenland Ice Sheet, J. Geophys. Res., 116, F04035, https://doi.org/10.1029/2010JF001934, 2011.

Howat, I. M., de la Peña, S., van Angelen, J. H., Lenaerts, J. T. M., and van den Broeke, M. R.: *Brief Communication* "Expansion of meltwater lakes on the Greenland Ice Sheet," The Cryosphere, 7, 201–204, https://doi.org/10.5194/tc-7-201-2013, 2013.

Huai, B., van den Broeke, M. R., Reijmer, C. H., and Noël, B.: A Daily 1-km Resolution Greenland Rainfall Climatology (1958–2020) From Statistical Downscaling of a Regional Atmospheric Climate Model, J. Geophys. Res. Atmos., 127, e2022JD036688, https://doi.org/10.1029/2022JD036688, 2022.

Lamarche-Gagnon, G., Wadham, J. L., Sherwood Lollar, B., Arndt, S., Fietzek, P., Beaton, A. D., Tedstone, A. J., Telling, J., Bagshaw, E. A., Hawkings, J. R., Kohler, T. J., Zarsky, J. D., Mowlem, M. C., Anesio, A. M., and Stibal, M.: Greenland melt drives continuous export of methane from the ice-sheet bed, Nature, 565, 73–77, https://doi.org/10.1038/s41586-018-0800-0, 2019.

Lampkin, D. J. and VanderBerg, J.: A preliminary investigation of the influence of basal and surface topography on supraglacial lake distribution near Jakobshavn Isbrae, western Greenland, Hydrol. Process., 25, 3347–3355, https://doi.org/10.1002/hyp.8170, 2011.

Law, R., Arnold, N., Benedek, C., Tedesco, M., Banwell, A., and Willis, I.: Over-winter persistence of supraglacial lakes on the Greenland Ice Sheet: results and insights from a new model, J. Glaciol., 66, 362–372, https://doi.org/10.1017/jog.2020.7, 2020.

https://doi.org/10.5194/egusphere-2026-6250
Preprint. Discussion started: 9 November 2026
© Author(s) 2026. CC BY 4.0 License.

Leeson, A. A., Shepherd, A., Briggs, K., Howat, I., Fettweis, X., Morlighem, M., and Rignot, E.: Supraglacial lakes on the Greenland ice sheet advance inland under warming climate, Nat. Clim. Change., 5, 51–55, https://doi.org/10.1038/nclimate2463, 2015.

Lüthje, M., Pedersen, L. T., Reeh, N., and Greuell, W.: Modelling the evolution of supraglacial lakes on the West Greenland ice-sheet margin, J. Glaciol., 52, 608–618, https://doi.org/10.3189/172756506781828386, 2006.

Lutz, K., Bever, L., Sommer, C., Seehaus, T., Humbert, A., Scheinert, M., and Braun, M.: Assessing supraglacial lake depth using ICESat-2, Sentinel-2, TanDEM-X, and in situ sonar measurements over Northeast and Southwest Greenland, The Cryosphere, 18, 5431–5449, https://doi.org/10.5194/tc-18-5431-2024, 2024.

Lutz, K., Tabone, I., Humbert, A., and Braun, M.: Multi-annual patterns of rapidly draining supraglacial lakes in Northeast Greenland, The Cryosphere, 19, 2601–2614, https://doi.org/10.5194/tc-19-2601-2025, 2025.

Melling, L., Leeson, A., McMillan, M., Maddalena, J., Bowling, J., Glen, E., Sandberg Sørensen, L., Winstrup, M., and Lørup Arildsen, R.: Evaluation of satellite methods for estimating supraglacial lake depth in southwest Greenland, The Cryosphere, 18, 543–558, https://doi.org/10.5194/tc-18-543-2024, 2024.

Morriss, B. F., Hawley, R. L., Chipman, J. W., Andrews, L. C., Catania, G. A., Hoffman, M. J., Lüthi, M. P., and Neumann, T. A.: A ten-year record of supraglacial lake evolution and rapid drainage in West Greenland using an automated processing algorithm for multispectral imagery, The Cryosphere, 7, 1869–1877, https://doi.org/10.5194/tc-7-1869-2013, 2013.

Musilova, M., Tranter, M., Wadham, J., Telling, J., Tedstone, A., and Anesio, A. M.: Microbially driven export of labile organic carbon from the Greenland ice sheet, Nature Geosci, 10, 360–365, https://doi.org/10.1038/ngeo2920, 2017.

Noël, B., van de Berg, W. J., van Wessem, J. M., van Meijgaard, E., van As, D., Lenaerts, J. T. M., Lhermitte, S., Kuipers Munneke, P., Smeets, C. J. P. P., van Ulft, L. H., van de Wal, R. S. W., and van den Broeke, M. R.: Modelling the climate and surface mass balance of polar ice sheets using RACMO2 – Part 1: Greenland (1958–2016), The Cryosphere, 12, 811–831, https://doi.org/10.5194/tc-12-811-2018, 2018.

Otosaka, I. N., Shepherd, A., Ivins, E. R., Schlegel, N.-J., Amory, C., van den Broeke, M. R., Horwath, M., Joughin, I., King, M. D., Krinner, G., Nowicki, S., Payne, A. J., Rignot, E., Scambos, T., Simon, K. M., Smith, B. E., Sørensen, L. S., Velicogna, I., Whitehouse, P. L., A, G., Agosta, C., Ahlstrøm, A. P., Blazquez, A., Colgan, W., Engdahl, M. E., Fettweis, X., Forsberg, R., Gallée, H., Gardner, A., Gilbert, L., Gourmelen, N., Groh, A., Gunter, B. C., Harig, C., Helm, V., Khan, S. A., Kittel, C., Konrad, H., Langen, P. L., Lecavalier, B. S., Liang, C.-C., Loomis, B. D., McMillan, M., Melini, D., Mernild, S. H., Mottram, R., Mouginot, J., Nilsson, J., Noël, B., Pattle, M. E., Peltier, W. R., Pie, N., Roca, M., Sasgen, I., Save, H. V., Seo, K.-W., Scheuchl, B., Schrama, E. J. O., Schröder, L., Simonsen, S. B., Slater, T., Spada, G., Sutterley, T. C., Vishwakarma, B. D., van Wessem, J. M., Wiese, D., van der Wal, W., and Wouters, B.: Mass balance of the Greenland and Antarctic ice sheets from 1992 to 2020, Earth Syst. Sci. Data., 15, 1597–1616, https://doi.org/10.5194/essd-15-1597-2023, 2023.

Pope, A., Scambos, T. A., Moussavi, M., Tedesco, M., Willis, M., Shean, D., and Grigsby, S.: Estimating supraglacial lake depth in West Greenland using Landsat 8 and comparison with other multispectral methods, The Cryosphere, 10, 15–27, https://doi.org/10.5194/tc-10-15-2016, 2016.

Qiu, J., Ran, J., Tangdamrongsub, N., Fettweis, X., Ali, S., Feng, W., and Wan, X.: Recent significant subseasonal fluctuations of supraglacial lakes on Greenland monitored by passive optical satellites, Remote Sens. Environ., 328, 114896, https://doi.org/10.1016/j.rse.2025.114896, 2025.

https://doi.org/10.5194/egusphere-2026-6250
Preprint. Discussion started: 9 November 2026
© Author(s) 2026. CC BY 4.0 License.



Tedesco, M., Lüthje, M., Steffen, K., Steiner, N., Fettweis, X., Willis, I., Bayou, N., and Banwell, A.: Measurement and modeling of ablation of the bottom of supraglacial lakes in western Greenland, Geophys. Res. Lett., 39, https://doi.org/10.1029/2011GL049882, 2012.

Tedesco, M., Willis, I. C., Hoffman, M. J., Banwell, A. F., Alexander, P., and Arnold, N. S.: Ice dynamic response to two modes of surface lake drainage on the Greenland ice sheet, Environ. Res. Lett., 8, 034007, https://doi.org/10.1088/1748-9326/8/3/034007, 2013.

The IMBIE Team: Mass balance of the Greenland Ice Sheet from 1992 to 2018, Nature, 579, 233–239, https://doi.org/10.1038/s41586-019-1855-2, 2020.

Thompson-Munson, M., Kay, J. E., and Markle, B. R.: Greenland's firn responds more to warming than to cooling, The Cryosphere, 18, 3333–3350, https://doi.org/10.5194/tc-18-3333-2024, 2024.

Trusel, L. D., Das, S. B., Osman, M. B., Evans, M. J., Smith, B. E., Fettweis, X., McConnell, J. R., Noël, B. P. Y., and van den Broeke, M. R.: Nonlinear rise in Greenland runoff in response to post-industrial Arctic warming, Nature, 564, 104–108, https://doi.org/10.1038/s41586-018-0752-4, 2018.

Wadham, J. L., Tranter, M., Skidmore, M., Hodson, A. J., Priscu, J., Lyons, W. B., Sharp, M., Wynn, P., and Jackson, M.: Biogeochemical weathering under ice: Size matters, Glob. Biogeochem. Cycles, 24, 2009GB003688, https://doi.org/10.1029/2009GB003688, 2010.

Wang, Y. and Sugiyama, S.: Supraglacial lake evolution on Tracy and Heilprin Glaciers in northwestern Greenland from 2014 to 2021, Remote Sens. Environ., 303, 114006, https://doi.org/10.1016/j.rse.2024.114006, 2024.

Wu, J., Zheng, L., Chen, Z., Zhou, Q., Peng, C., Liang, Q., Li, T., Huai, B., Sun, W., Cheng, X., Law, R., and Hui, F.: Greenland supraglacial lakes albedo-depth parameterization from multi-source remote sensing: An application of lake-albedo feedback modeling, J. Hydrol., 662, 134001, https://doi.org/10.1016/j.jhydrol.2025.134001, 2025.

Wu, J., Zheng, L., Liang, Q., Li, T., Zhou, Q., Peng, C., Huai, B., Chen, Z., Cheng, X., and Hui, F.: Distributed modeling reveals the evolution of supraglacial lakes: a multi-basin study on the Greenland ice sheet, J. Hydrol., 680, 136548, https://doi.org/10.1016/j.jhydrol.2026.136548, 2026.

Yang, K., Smith, L. C., Fettweis, X., Gleason, C. J., Lu, Y., and Li, M.: Surface meltwater runoff on the Greenland ice sheet estimated from remotely sensed supraglacial lake infilling rate, Remote Sens. Environ., 234, 111459, https://doi.org/10.1016/j.rse.2019.111459, 2019.

Zhang, Q., Ding, M., Van Den Broeke, M. R., Noël, B., Fettweis, X., Wang, S., Sun, W., You, Q., Xiao, C., Qin, D., and Huai, B.: Variations in Greenland surface melt and extreme events from 1958 to 2023, Adv. Clim. Change Res., S1674927825001170, https://doi.org/10.1016/j.accre.2025.05.004, 2025.

Zheng, L., Shang, X., van den Broeke, M. R., Noël, B., Li, X., Fettweis, X., Liang, Q., Wang, K., Liu, J., and Cheng, X.: Rapid increases in satellite-observed ice sheet surface meltwater production, Nat. Clim. Chang., 15, 769–774, https://doi.org/10.1038/s41558-025-02364-4, 2025.

Zhou, Q., Liang, Q., Xiao, W., Li, T., Zheng, L., and Cheng, X.: Supraglacial Lake Depth Retrieval from ICESat-2 and Multispectral Imagery Datasets, J. Remote Sens., 5, 0416, https://doi.org/10.34133/remotesensing.0416, 2025.